

# MULTIPHYSICS SIMULATIONS OF THE WIDE OPENED WAVEGUIDE CRAB-CAVITY

K. Papke\*, A. Amorim Carvalho, A. Grudiev, and C. Zanoni  
 CERN, Geneva, Switzerland

## Abstract

In the frame of a FCC study, a first prototype of a compact superconducting crab-cavity, using Nb-on-Cu-coating technique is being manufactured and investigated. The design, which is based on the ridged waveguide resonator, is subjected to multipacting and pressure sensitivity simulations. First results of these simulations are presented and compared to those of other SRF cavities. Furthermore, several aspects related to the design of the fundamental mode coupler and HOM dampers are presented.

## INTRODUCTION

The study about a compact superconducting crab-cavity for LHC using Nb-on-Cu-coating techniques [1], launched in 2014 has been recently accepted for a FCC work package at CERN. In contrast to the Double Quarter Wave (DQW), Four-Road, and RF Dipole [2], the design of the cavity which we denote as Wide Opened Waveguide Crab Cavity (WOWCC) is based on a ridged waveguide resonator with wide open apertures to allow direct access to the interior for the surface preparation and coating (Fig. 1). Noteworthy, that due to the large apertures, the number of trapped higher order modes (HOMs) is comparably low which eventually facilitates their damping. Likewise, the longitudinal and transverse impedances are lower than those of the other three crab cavities. It should be mentioned that a similar design called Quasi-waveguide Multicell Resonator (QMIR) is being studied and developed at FermiLab for the Advanced Photon Source's Short Pulse X-ray project [3]. However, the QMiR is machined out of bulk niobium. We omit the motivation of thin-film against bulk niobium superconducting cavities since it has been addressed in [1].

The WOWCC will be operated with a frequency of 400 MHz at 4.5 K, providing a deflecting voltage of 3 MV over an effective length of 1 m with a total RF power loss of approximately 60 W. The main parameter are listed in Table 1.

In this paper, we follow up the studies presented in [1]. These involve the power loss and Q factor calculations incorporating a field dependent localized surface resistance and the frequency sensitivity against pressure fluctuations by means of coupled 3D RF and structural mechanics simulations. Further detailed calculations of the longitudinal and transverse impedances are compared to those of the DQW and the RF Dipole crab cavity. Moreover, the fundamental mode coupler and HOM antennas are addressed as well as the multipacting in the bare cavity.

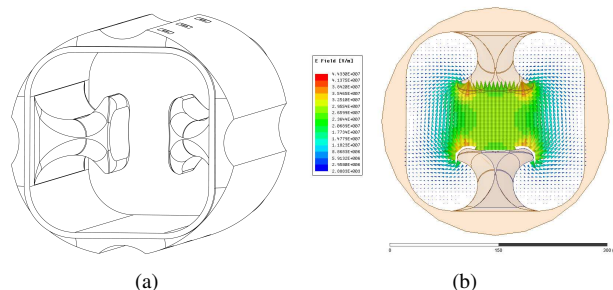


Figure 1: (a) Center part of the Wide Opened Waveguide Crab Cavity (WOWCC). (b) The electric field between the two mushroom-shaped ridges in the cavity center.

Table 1: Main Parameters of the WOWCC

Parameter	Unit	Value
dimensions (W×H×L)	[mm]	250×250×1400
smallest aperture	[mm]	42
frequency	[MHz]	400
geometry factor G	[Ω]	108.9
deflecting voltage $V_{x0}$	[MV]	3.0
$R_x/Q$	[Ω]	343.5
$E_{pk}$ at $V_{x0}$	[MV/m]	45.3
$B_{pk}$ at $V_{x0}$	[mT]	78.3
$Q_0$ at $V_{x0}$		$4.0 \times 10^8$

## RF DESIGN

The design process has been subjected to the following requirements exhaustively discussed in [1]:

- Facilitate the access for sputtering cathodes.
- The Frequency is fixed to 400 MHz.
- Minimum aperture is 42 mm.
- Minimize surface peak fields with respect to  $V_{x0}$ .
- Minimize sextupolar component  $b_3/V_{x0}$  [4].

In the following, we assess further RF characteristics of the optimized design or complete earlier studies, respectively.

### RF Power Loss Calculation at 4.5 K

We further refined the procedure outlined in [1] to evaluate the dissipating power in the cavity wall  $P_{diss}$  as follows: (i) Calculate the RF field and surface loss density assuming a homogenous surface resistance of copper at 300 K<sup>1</sup>. (ii) Rescale locally the surface resistance taking into account the magnetic field  $B_s$  (Fig. 2) to obtain the total power loss

<sup>1</sup> The calculations are done using HFSS [5].

\* kai.papke@cern.ch

Content from this work may be used under the terms of the CC BY 3.0 licence (© 2017). Any distribution of this work must maintain attribution to the author(s), title of the work, publisher, and DOI.

for niobium at 4.5 K. The latter is based on an exponential fit gained from the measurements at 4.5 K done for the LHC accelerating cavities [6]:

$$R_s^{\text{LHC}}[\text{n}\Omega] = 54.7 + 19.0 \exp(54B_s[\text{T}]) \quad (1)$$

However, we do not apply (1) directly for the scaling of the localized surface loss density since it represents the surface resistance averaged over the entire cavity surface. Instead, we have chosen the same approach for the localized surface resistance with yet unknown coefficients and proceed iteratively using the steps (i) and (ii) in order to successively approach the averaged and measurable field dependent surface resistance given in (1). The coefficients converged after five to ten iterations and are close to the values in (1). The resulting intrinsic quality factor of  $4 \times 10^8$  is slightly lower than those evaluated in [1] as shown in Table 2.

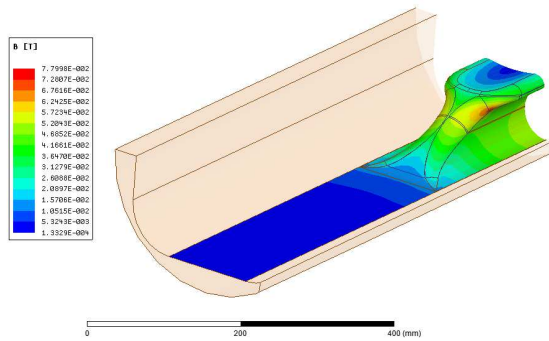


Figure 2: Magnetic field at the cavity surface.

Table 2: Loss and  $Q_0$  Calculations

Method	$P_{\text{diss}}$	$Q_0$
homogenous surface resistance of 250 n $\Omega$ [1]	60 W	$4.3 \times 10^8$
localized scaling of the surface loss density by (1) [1]	57 W	$4.6 \times 10^8$
iterative procedure to recover (1) as average over the cavity surface	65 W	$4.0 \times 10^8$

### Beam-coupling Impedance

The smooth 30-degree tapers and the large cross-section beam pipes provide naturally efficient HOM damping and low beam coupling impedance as shown Table 3 by means of the effective longitudinal and transverse impedances [7]. The WOWCC roughly provides half the impedance of the DQW and only a third of the RF Dipole crab cavity, both longitudinally and transversely. The evaluation is based on wakefield simulations using CST [8] assuming a bunch length with RMS sigma of  $\sigma_z = 80$  mm in correspondence to LHC. Noteworthy, that the fundamental mode coupler considered in the next section has only a marginally effect on the impedance of the WOWCC. While the longitudinal

Table 3: Effective Impedances of Crab Cavities

Cavity	$(Z_{\parallel}/n)_{\text{eff}}$ [m $\Omega$ ]	$(Z_x)_{\text{eff}}$ [k $\Omega$ ]	$(Z_y)_{\text{eff}}$ [k $\Omega$ ]
WOWCC	0.973	1.574	0.434
DQW	1.960	3.381	2.331
RF Dipole	2.554	5.234	2.253

impedance increases by 2-5 %, the transverse impedance decreases by 10-30 % depending on the coupler dimensions. The HOM dampers and eventual tapers towards the beam pipe are not included in the impedance calculations and left for the future work.

A first estimate of maximum feasible external quality factors  $Q_{\text{ext}}$  for HOMs is shown in Table 4. The values are based on the impedance constraints of HL-LHC [9] as well as the loss or kick factors of the longitudinal and transverse wake potentials, respectively.

Table 4: Max. Required  $Q_{\text{ext}}$  based on HL-LHC Data [9]

Mode type	Peak Real Impedance	$Q_{\text{ext}}$ threshold
Monopole	2.4 M $\Omega$	$4.04 \times 10^5$
Dipole	1.5 M $\Omega$ /m	$6.56 \times 10^3$

### Fundamental Mode Coupler

In contrast to the DQW or RF Dipole crab cavities, the fundamental mode is coupled via the electric field in the deflecting plane close to the taper (Fig. 3). A simpler probe antenna can be used instead of a hook antenna which is likewise favored from the thermal point of view. The optimal coupling is derived from the input power required to compensate the beam loading assuming an off-centered beam by  $\pm 2$  mm in the worst case (Fig. 4). The minimum appears at around  $Q_{\text{ext}} = 1 \times 10^6$  providing a slightly lower coupling than considered for the other crab cavities due to their higher  $R/Q$  values [9].

Three different probe antennas denoted to as C1, C2, and C3 are compared in Table 5, each of them adjusted to a coupling of  $Q_{\text{ext}} = 1 \times 10^6$ . The first two agree in their dimensions with those used for the accelerating cavities in LHC or SPL [10], respectively. The latter is originated from

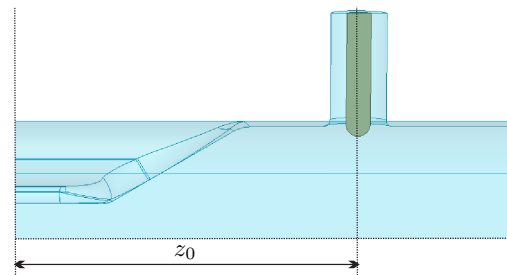


Figure 3: Fundamental mode coupler in the deflecting plane close to the 30 deg taper.

Content from this work may be used under the terms of the CC BY 3.0 licence (© 2017). Any distribution of this work must maintain attribution to the author(s), title of the work, publisher, and DOI.

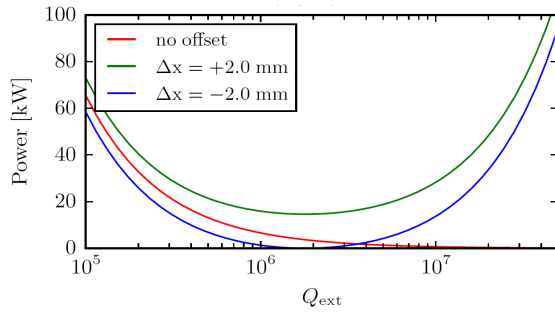


Figure 4: RF Power as a function of the external quality factor  $Q_{ext}$  for different beam offsets.

the fundamental mode coupler of the DQW crab cavity, by removing the hook.

Table 5: Properties of Fundamental Mode Couplers

Parameter	Unit	C1	C2	C3
inner diameter	[mm]	41.0	43.0	27.0
outer diameter	[mm]	145.0	100.0	62.0
insertion	[mm]	0.0	0.0	8.0
$z_0$	[mm]	467	429	375
$E_{pk}$ at $V_{x0}$	[kV/m]	0.169	0.217	0.600
$B_{pk}$ at $V_{x0}$	[mT]	0.35	0.54	1.22

The cavities' dipolar and sextupolar components are not influenced by the fundamental mode coupler as it can be seen in Table 6. Only a skew quadrupolar component  $a_2$  is introduced, however its value is marginal.

Table 6: Multipolar Moments with and without Fundamental Mode Coupler at the Specified Deflecting Voltage of 3 MV/m

	Unit	No coupler	C1	C3
$b_1$	[T m]	$3.1 \times 10^{-3}$	$3.1 \times 10^{-3}$	$3.1 \times 10^{-3}$
$a_2$	[Tm/m]	–	$3.5 \times 10^{-5}$	$8.0 \times 10^{-6}$
$b_3$	[Tm/m <sup>2</sup> ]	$8.2 \times 10^{-3}$	$8.2 \times 10^{-3}$	$8.3 \times 10^{-3}$

In agreement with the power requirements of the DQW and RF Dipole crab cavities, the smallest coupler (C3) has been selected which is also favored from the mechanical point of view. The higher surface peak fields at the antenna tip are acceptable but must be carefully taken into account for the engineering design. Furthermore, this coupler introduces the fewest asymmetric HOMs.

### HOM Damping

Very few modes below 2.5 GHz have been identified by eigenmode simulations using CST and HFSS as listed in Table 7. Modes above this frequency are expected to propagate out in accordance with the analysis of the beam coupling impedance [1]. Besides there is one asymmetric HOM at

Table 7: HOMs of the WOWCC

Cavity mode <sup>a</sup>	$f$ [MHz]	$R/Q$ [ $\Omega$ ] <sup>b</sup>	Beam pipe mode <sup>a</sup>	Cut-off [MHz]	$Q_{ext}$ <sup>c</sup>
TE <sub>111</sub>	400.0	342.7	TE <sub>11</sub>	624.9	$1.0 \times 10^6$
TE <sub>112</sub>	638.3	15.7	TE <sub>11</sub>	624.9	< 35
TE <sub>111</sub>	643.8	0.08	TE <sub>11</sub>	624.9	< 40
TE <sub>012</sub>	667.0	13.9	TM <sub>01</sub>	847.6	$4.8 \times 10^4$
TM <sub>011</sub>	827.2	25.1	TM <sub>01</sub>	847.6	$4.8 \times 10^3$
TE <sub>211</sub>	1276	0.30	TE <sub>21</sub>	1180	$2.3 \times 10^4$

<sup>a</sup> Mode indices correspond to circular waveguide modes.

<sup>b</sup> For monopole modes, the longitudinal  $R/Q$  is calculated while for dipole modes, the transverse  $(R/Q)_{\perp}$ , both in linac definition.

<sup>c</sup> Incorporates the damping via the wide opened apertures, the fundamental mode coupler and the two HOM probe antennas (Fig. 5).

540 MHz due to the fundamental mode coupler which should be considered in its detailed RF design.

Naturally the quadrupolar modes are harmless for the beam stability. Likewise the first higher order dipole modes are of less concern since they propagate out and can be handled eventually by HOM dampers outside of the cryo module. Both monopole modes at 667 and 827 MHz can be sufficiently damped by probe antennas perpendicular to the fundamental mode coupler as shown in Fig. 5. At this loca-

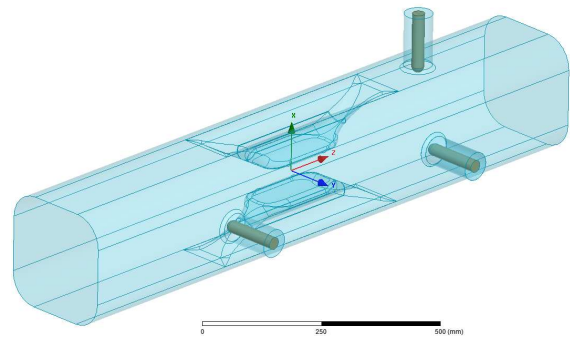


Figure 5: Cavity with the fundamental mode coupler (at the top) and two HOM couplers where the field of the fundamental mode vanishes.

tion the field of the fundamental mode vanishes such that a notch filter is not required. The remaining TE<sub>211</sub> dipole mode at 1276 MHz is partially damped via the wide opened apertures but not sufficiently with respect to the requirements in Table 4. A HOM coupler with notch filter might be considered in the future if the impedance constraints are maintained or even stronger for FCC. The current results of HOM damping in terms of  $Q_{ext}$  are listed in Table 7.

### Multipacting

The multipacting has been characterized using both, CST<sup>2</sup> and ACE3P<sup>3</sup> [11]. In CST, typically, the electron growth

<sup>2</sup> Eigenmode solver of CST MWS combined with the particle-in-cell (PIC) solver of CST PS

<sup>3</sup> Omega3P combined with Track3P

rate is analyzed either explicitly by the ratio of secondary emitted electrons to the primary electrons:

$$\text{growth rate} = \frac{I_{\text{SEE}}}{I} \quad (2)$$

or implicitly by an exponential fit of the total electron number over the time according to:

$$\frac{I(t_2)}{I(t_1)} = \text{growth rate}^{(2f\Delta t/n)}, \quad (3)$$

where  $n$  corresponds to the order of multipacting. In ACE3P, the impact energy of resonant particles is compared to the energy range in which the material dependent secondary electron yield (SEY) is larger than one. For niobium, this range lies approximately between 80 and 2000 eV but the actual SEY curve strongly depends on the surface preparation. The SEY of niobium after 300 °C bake taken from the material library of CST serves as a reference in the following.

To keep the required computing resources for both tracking codes feasible, the cavity wall was partitioned into six slices along the longitudinal direction to localize the initial particle emission (Fig. 6). The particles were tracked over 70 RF cycles in ACE3P and 10 to 100 RF cycles in CST depending on the growth rate.

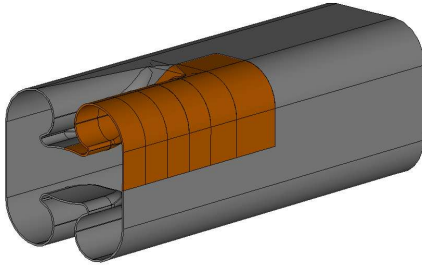


Figure 6: The partition of the cavity surface to provide local initial field emission.

Three multipacting barriers between 0.2 and 2 MV deflecting voltage have been identified using ACE3P (Figs. 7 and 8). According to the Grapunov-Miller force, the resonant particles trajectories appear at distinct electric field minima which becomes obvious by observing the rescale field plot in Fig. 7 (a). The first barrier at field level of  $V_x = 0.2 - 0.7$  MV is driven by resonant particles between the two ridges close to the cavity center. Likewise close to the center but at the top and bottom appears multipacting at  $V_x = 1 - 1.5$  MV causing the second barrier whereas an electron growth further away from the ridges create a third barrier at even higher field level.

CST provides similar results based on the electron growth rate as shown in Fig. 9 again for different localized initial particle emitters. However, the second and third barriers are significantly larger whereas the first one is slightly smaller. Using the SEY of argon treated niobium [8] which provides a lower peak value, the sizes of the second and third barriers somewhat reduces but qualitatively remain. The first

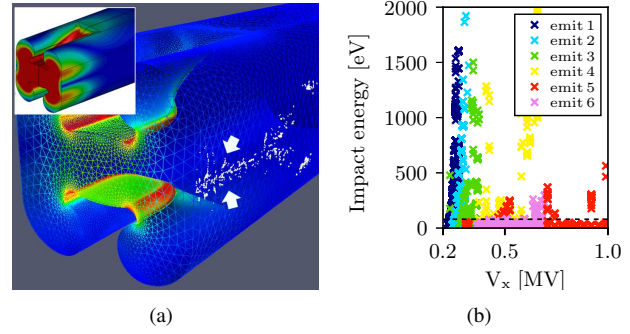


Figure 7: First multipacting barrier at  $V_x = 0.2 - 0.7$  MV. (a) Electric field at the cavity surface with the resonant particles trajectories after 70 RF cycles (white). (b) Corresponding impact energies for different emitter locations.

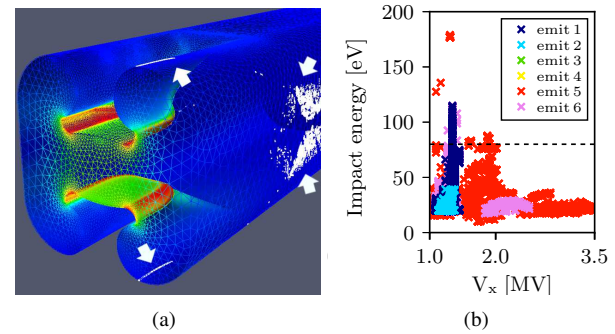


Figure 8: Second and third barrier at  $V_x = 1 - 2$  MV. (a) Electric field at the cavity surface with the resonant particles trajectories after 70 RF cycles (white). (b) Corresponding impact energies for different emitter locations.

barrier disappears. It is noteworthy that the RF Dipole crab cavity provides comparable multipacting barriers according to ACE3P simulations but during the first cold test only the narrower barrier at the lowest field level appeared which could successfully passed [12].

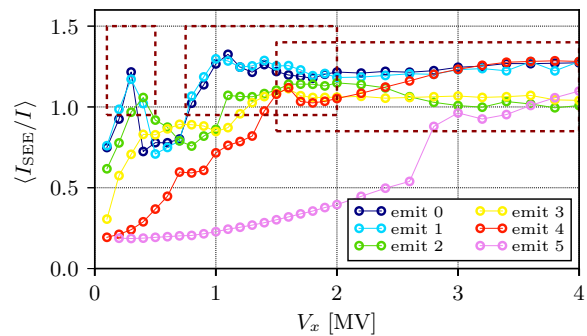


Figure 9: Electron growth rate derived from CST PIC simulations for different emitter locations. The three multipacting barriers are highlighted in dashed red.

## ENGINEERING DESIGN

A first prototype is being fabricated following the concept presented in [1]. The thickness and, hence, the weight of the cavity was reduced in order to facilitate the handling during cleaning, surface preparation or coating.

### RF Sensitivity to Pressure

Early estimations showed that the cavity is highly sensitive to pressure. In order to mitigate this aspect, the outer cavity shape is optimized such that the deformation due to pressure fluctuations affects the fundamental mode frequency as less as possible. It is worth noting that the dynamic contribution is considered quasi-static.

The external shape is parametric in  $r_1$ , which is the radius of the outer groove in Fig. 10 (a). In the beginning, two

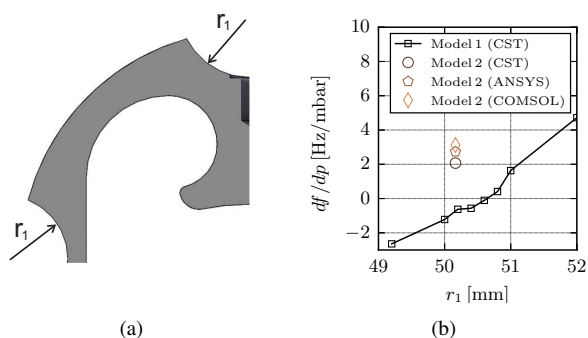


Figure 10: (a) Quarter of the cavity cross section with the free parameter  $r_1$ . (b) The frequency versus pressure sensitivity as a function of  $r_1$ . Model 1 is a former version of the prototype. Model 2 corresponds to the prototype.

different radii for the horizontal and vertical grooves were foreseen which could be simplified to a common one in the frame of optimizations. In contrast to [1], the RF simulation is fully coupled to the structural mechanics simulation, meaning that the eigenmode simulation is carried out directly on the deformed geometry using three codes: CST<sup>4</sup>, ANSYS<sup>5</sup>, and COMSOL [13].

The largest deformation appears at the welding location, where the thickness is the smallest, Fig. 11. It should be noted that the resulting deformations in CST are higher by 5-10% than in the other codes. This aspect has been confirmed by the CST support but not resolved yet. In light of these uncertainties, a pressure sensitivity of the first prototype with  $r_1 = 50.164$  mm is expected to be in a range of 2 to 4 Hz/mbar (Model 2 in Fig. 10).

All the software packages have significant drawbacks that makes hard the estimation of the sensitivity with a bit of statistics. The plan is to refine one or more methods and estimate the pressure sensitivity accounting for the variability

<sup>4</sup> Eigenmode solver of CST MWS and structural mechanics solver of CST MP

<sup>5</sup> HFSS with ANSYS

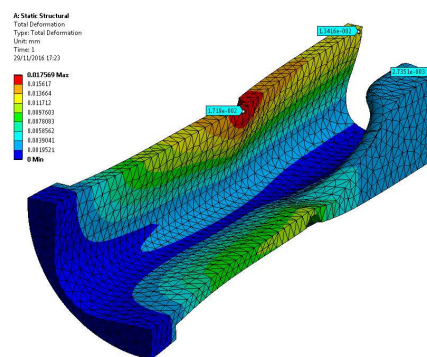


Figure 11: Deformation due to a quasi-static pressure difference at the cavity walls of 1 bar as simulated in ANSYS.

of the main parameters (e.g. material properties, geometrical tolerances) and then compare it with the results of the vertical cold test.

## CONCLUSIONS AND OUTLOOK

The design of the WOWCC has been optimized taking into account RF performance, mechanical constraints and the feasibility for surface coating. Former studies assessed the thermal behavior. Multipacting barriers are very likely to appear in the cold test. The first prototype is under fabrication at CERN.

## REFERENCES

- [1] A. Grudiev *et al.*, in *Proc. SRF2015*, 2015, paper THPB048.
- [2] S. D. Silva *et al.*, “Superconducting RF-Dipole Deflecting and Crabbing Cavities,” in *Proc. SRF2013*.
- [3] A. Lunin *et al.*, *Physics Procedia*, vol. 79, pp. 54 – 62, 2015.
- [4] J. Barranco García *et al.*, *Phys. Rev. Accel. Beams*, vol. 19, p. 101003, Oct 2016.
- [5] *HFSS - Ver. 2014*, ANSYS Inc., Canonsburg, USA, 2014.
- [6] S. Bauer *et al.*, in *Proc. 1999 Workshop on Superconductivity*, 1999, paper WEP016.
- [7] F. Ruggiero, Tech. Rep. CERN-SL-95-09-AP, 1995. [Online]. Available: <https://cds.cern.ch/record/279204>
- [8] *CST - Ver. 2016*, CST AG, Darmstadt, Germany, 2016.
- [9] R. Calaga, “Crab Cavities for the LHC Upgrade,” 2012, presented at the Workshop on LHC Performance, Chamonix.
- [10] F. Gerigk *et al.*, *Conceptual Design of the Low-Power and High-Power SPL*. CERN, 2014.
- [11] K. Ko and A. Candel, “Advances in Parallel Electromagnetic Codes for Accelerator Science and Development,” in *Proc. LINAC2010*, 2010, paper FR101.
- [12] D. Silva *et al.*, *Phys. Rev. ST Accel. Beams*, vol. 16, p. 082001, Aug 2013.
- [13] *COMSOL - Ver. 5.2a*, Comsol Multiphysics GmbH, Göttingen, Germany, 2016.